

Charges for Large Scale Binding Free Energy Calculations with the Linear Interaction Energy Method

Göran Wallin,[†] Martin Nervall,[†] Jens Carlsson, and Johan Åqvist*

*Department of Cell and Molecular Biology, Uppsala University,
Box 596, SE-751 24 Uppsala, Sweden*

Received September 26, 2008

Abstract: The linear interaction energy method (LIE), which combines force field based molecular dynamics (MD) simulations and linear response theory, has previously been shown to give fast and reliable estimates of ligand binding free energies, suggesting that this type of technique could be used also in a high-throughput fashion. However, a limiting step in such applications is the assignment of atomic charges for compounds that have not been parametrized within the given force field, in this case OPLS-AA. In order to reach an automatable solution to this problem, we have examined the performance of nine different *ab initio* and semiempirical charge methods, together with estimates of solvent induced polarization. A test set of ten HIV-1 reverse transcriptase inhibitors was selected, and LIE estimates of their relative binding free energies were calculated using the resulting 23 different charge variants. Over 800 ns of MD simulation show that the LIE method provides excellent estimates with several different charge methods and that the semiempirically derived CM1A charges, in particular, emerge as a fast and reliable alternative for fully automated LIE based virtual screens with the OPLS-AA force field. Our conclusions regarding different charge models are also expected to be valid for other types of force field based binding free energy calculations, such as free energy perturbation and thermodynamic integration simulations.

Introduction

Computational structure-based ligand design relies on accurate predictions of binding free energies of usually relatively small organic molecules upon binding to a macromolecular receptor. These predictions can then serve as guidelines for lead compound identification and optimization. The methods used in structure-based binding affinity prediction range between being theoretically stringent to more or less approximate, where there is always a tradeoff between accuracy and computational cost. For instance, free energy perturbation (FEP) is one of the rigorous but more time-consuming methods that often requires considerable initial preparation by the user followed by days of calculation. If infinite thermodynamic sampling could be attained, the method would in principle deliver the true binding free

energies given by the particular potential energy function. However, the limited sampling that can be achieved by computer simulations remains a serious problem, and this is the main reason why FEP applications are still rare in structure-based ligand design. In contrast, empirical scoring functions are much faster, typically requiring only fractions of a second per binding estimate, but then only because they describe ligand-protein interactions phenomenologically and usually do not rely on conformational sampling at all. In between these extremes there is a wide range of methods, reviewed in refs 1–3, and one of these is the linear interaction energy (LIE) method which is the focus of the present work.

The LIE method is a semiempirical approach which is faster than free energy perturbation, typically requiring a few hours per binding estimate, yet is more accurate than empirical scoring functions and has been employed for a number of biomolecular systems with good results.^{1,4–9} The approximations behind the LIE method, namely electrostatic

* Corresponding author phone: +46 18 471 4109; fax: +46 18 53 69 71; e-mail: aqvist@xray.bmc.uu.se.

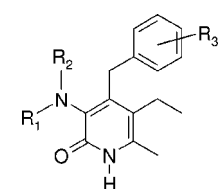
[†] These authors contributed equally to this work.

linear response together with a nonpolar binding contribution that depends linearly on ligand size (representing hydrophobic effect, translational/rotational entropy loss, etc.),¹⁰ leads to a simple linear relation between the binding free energy and the difference in ligand-surrounding average potential energies between the bound and free states, i.e. between the compound immersed in water and enveloped in the binding pocket. These average energies are then calculated as arithmetic mean values from sufficiently long molecular dynamics (MD) or Monte Carlo runs. With continuously increasing computational power, the limiting step of free energy calculations with the LIE method has shifted from the actual simulations to system preparation and analysis. Hence, whereas LIE can conveniently handle hundreds of compounds today, the preparation process needs to be fully automated to further push this number to the tens or hundreds of thousands of compounds that will be computationally feasible in a not too distant future. At this point, our standard LIE scheme has recently been applied to screen about 1000 commercially available compounds for inhibitory activity against a potential drug target in tuberculosis, the 1-deoxy-D-xylulose-5-phosphate reductoisomerase, with promising results (Carlsson et al., unpublished). An efficient simplified LIE version based on energy minimization with a continuum solvent model, rather than explicit water simulations, has also been devised by Caffisch and co-workers and successfully applied for virtual screening on the order of 10⁵ compounds.^{11,12}

One of the major bottlenecks in the preparation process is the derivation and assignment of partial charges, and solvation free energies of organic compounds are clearly affected by this choice.^{13,14} It is therefore of considerable interest to automate this process, and, herein, we investigate the precision and accuracy of several different charge schemes for use together with the OPLS-AA force field. These models include rigorous *ab initio* schemes (Mulliken,¹⁵ Natural Population Analysis,¹⁶ Atoms in Molecules topological analysis,^{17,18} and ESP methods by Breneman¹⁹ and Merz–Kollman–Singh²⁰) as well as two fast parametrized methods, one based on semiempirical wave functions (CM1A²¹ and its scaled version CM1A*1.14) and one on the concept of electronegativity equalization (Vcharge²²). The relative performance of the different schemes is evaluated with respect to ligand binding free energies as given by LIE and is compared to the standard charge method associated with the force field, in this case a simple rule based method of combining OPLS-AA fragments. In addition, the effect of solvent charge polarization on the *ab initio* wave functions is evaluated through the Conductor-like Polarizable Continuum Model (CPCM).²³

Our main goal is thus to investigate whether there are readily automatized charge schemes that can be used in conjunction with the OPLS-AA force field for large scale binding free energy calculations, to eliminate the need for manual parametrization of new chemical structures or fragments. To this end, ten HIV-1 reverse transcriptase (RT) inhibitors were selected from a previous study by Carlsson et al.,²⁴ such that they span the relative ligand binding free energy space and provide reliable results from well con-

Table 1. HIV-1 Reverse Transcriptase Inhibitors Used in This Work^a



	R ₁	R ₂	R ₃	IC ₅₀
39	CH ₃	C ₃ H ₇	3,5-diCH ₃	0.016
40	CH ₃	CH(CH ₃)CH ₂ OCH ₃	3,5-diCH ₃	0.006
41	CH ₃	(CH ₂) ₃ SCH ₃	3,5-diCH ₃	0.025
46	H	COC ₃ H ₇	3,5-diCH ₃	100
49	H	C ₄ H ₉	3,5-diCH ₃	0.126
52	H	CH ₂ C ₆ H ₅	3,5-diCH ₃	0.251
60	CH ₃	(CH ₂) ₃ OH	3-CH ₃	0.003
62	CH ₃	(CH ₂) ₂ OCH ₃	3-CH ₃	0.001
65	CH ₃	(CH ₂) ₂ CN	3-CH ₃	0.016
68	H	NH-CS-NHC ₆ H ₅	3-CH ₃	3.162

^a Their experimental IC₅₀ values (μM) as well as their naming have been adopted from ref 25.

verged runs with LIE and OPLS-AA. These compounds consist of a pyridinone ring connected to a benzyl group, with two side chains differing along the ligand series (see Table 1).

Methods

The ten RT ligands were selected from a previously published inhibitor series²⁵ and span 5 orders of magnitude in terms of experimentally observed IC₅₀-values. The inhibitor-enzyme structures were adopted from earlier work²⁴ and originate from dockings with GOLD²⁷ that were carried out on a crystal structure²⁶ of HIV-1 RT in complex with compound **62** studied here (PDB code: 2BAN). MD simulations were conducted with the Q software package²⁸ in an 18 Å sphere centered on the inhibitor, using the OPLS-AA force field.²⁹ The three docked conformations with the highest ranking for each ligand were extracted and solvated with TIP3P waters.³⁰ The solvated systems were heated to 310 K in six consecutive steps, while at the same time releasing positional restraints applied to the heavy atoms of the enzyme. An equilibration phase of 50 ps was performed with no positional restraints before entering the collection phase, which was pursued for 1 ns with a time step of 1 fs. Since the ligand simulations in the free state converged much faster, a single simulation of 500 ps was considered to be sufficient for each ligand, thus yielding a total simulation time of 3.5 ns for each ligand. Given that there were ten ligands and that 23 distinct sets of partial charges were examined for each of them, this added up to a total simulation time of about 800 ns. During the collection phase ligand-surrounding energies were collected every 50 fs. The internal geometries of all solvent molecules were constrained with the SHAKE algorithm,³¹ and the SCAAS model^{28,32} was applied to solvent molecules close to the border to model the density and dipole angular distribution of bulk water. The nonbonded cutoff was set to 10 Å for all atoms inside the sphere, except for ligand atoms for which all nonbonded

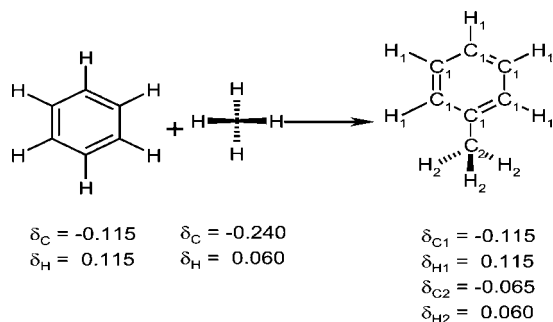


Figure 1. Example of the OPLS-AA fragment based charge model, where a benzene and a methyl group are merged to form a toluene. The partial charges of all atom types in each molecular species are displayed under the corresponding molecule. The ambiguities that arise when the two groups are merged are dealt with by adjusting the charge of the aliphatic carbon (C_2) in the toluene molecule.

interactions were explicitly calculated. Long-range electrostatic interactions were treated with the local reaction field multipole expansion approximation,³³ whereas atoms outside the simulation sphere, which only interacted through bonded terms, were subjected to strong positional restraints.

Linear Interaction Energy. In the LIE method, the binding free energy is estimated in analogy with solvation energies as the free energy of transfer between water and protein environments. Simulations are carried out for the ligand in water and in the solvated protein, and the Gibbs free energy of binding is calculated from the ligand-surrounding (*l-s*) electrostatic (*el*) and van der Waals (*vdW*) interaction energies through the LIE equation

$$\Delta G_{bind}^{LIE} = \alpha \Delta \langle U_{l-s}^{vdW} \rangle + \beta \Delta \langle U_{l-s}^{el} \rangle + \gamma \quad (1)$$

where the Δ 's refer to differences in protein and water simulations. While the $\beta \Delta \langle U_{l-s}^{el} \rangle$ term represents the polar contribution to the binding free energy and is based on a linear response approximation, $\alpha \Delta \langle U_{l-s}^{vdW} \rangle + \gamma$ represents the nonpolar binding contributions. The latter term can be derived from the observation that both nonpolar solvation energies in different solvents and ligand-surrounding van der Waals interactions tend to scale linearly with solute size measures, such as molecular surface area or the number of heavy atoms in the ligand.^{7,10} This leads to the following type of relationship between $\Delta \langle U_{l-s}^{vdW} \rangle$ and the change in nonpolar solvation free energy, $\Delta \Delta G_{sol}^{np}$, between protein and water environments

$$\begin{aligned} \Delta \Delta G_{sol}^{np} &= a\sigma + b \\ \Delta \langle U_{l-s}^{vdW} \rangle &= c\sigma + d \\ \Rightarrow \Delta \Delta G_{sol}^{np} &= \frac{a}{c} (\Delta \langle U_{l-s}^{vdW} \rangle - d) + b = \alpha \Delta \langle U_{l-s}^{vdW} \rangle + \gamma \quad (2) \end{aligned}$$

where σ is a size measure, and a , b , c , and d are empirically derived parameters. From eq 2, the contributions from nonpolar solvation to α and γ in eq 1 can in principle be identified as a/c and $b-ad/c$, respectively. Since our standard parametrization of LIE was performed using experimental binding free energies, the obtained value of $\alpha = 0.18$ takes all size dependent contributions to binding into account, such as the hydrophobic effect and relative translational and

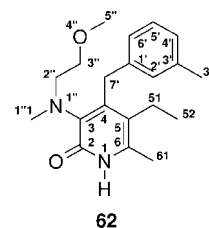


Figure 2. Chemical structure formula for compound 62.

rotational entropies as well as van der Waals interactions. The constant offset γ has been shown to correlate with the hydrophobicity of the binding site pocket⁵ and is thus generally protein specific but is freely optimized here for each charge set since only relative binding free energies can be extracted from the present experimental data.²⁴

In our standard version of the LIE method, the ligand-surrounding electrostatic energies in both the protein and water simulations are scaled by the same factor, which assumes that the electrostatic response of the protein binding site is similar to that of water. The value of the β coefficient can be derived from linear response approximation, which predicts that $\beta = 0.5$.³⁴ However, based on rigorous FEP calculations in different solvents carried out by Åqvist and Hansson³⁴ (see also ref 5), the β value used for a ligand in the standard parametrization of the LIE method, β_{FEP} , is determined by its chemical groups. For the inhibitors studied here β_{FEP} is equal to 0.43 in all cases except for compound 60 (for which $\beta_{FEP} = 0.37$).³⁵ Since the point of this study is to examine the impact of charge variation on the LIE method, and the α - and β -values have been shown⁵ to provide consistent results even with different force fields (Amber95, Gromos87, and OPLS-AA), this standard model with $\alpha = 0.18$ was adopted, and γ was optimized for every charge set.

Partial Charges. Since partial atomic charges are not quantum mechanical observables and therefore cannot be measured by experiment, there is no unambiguous way of assigning them. In this study a few acknowledged methods have been chosen which will be briefly outlined below.

In the *ab initio* Mulliken population analysis,¹⁵ the total molecular wave function is subdivided into net atomic and overlap populations, where the overlap populations are evenly distributed between the atoms. The Mulliken population of an atom A is thus given by the diagonal sum $n_A = \sum_{\mu \in A} (PS)_{\mu\mu}$ where P and S denote the density and overlap matrix, respectively. The partial charge is then simply the difference between the atomic population and the nuclear charge. Although simple and straightforward, this scheme is overly basis set dependent, especially when compared to actual differences in the wave function.³⁶

In contrast, the Natural Population Analysis (NPA) by Weinhold et al.¹⁶ transforms the generally nonorthogonal basis set into an orthonormal basis of atomic orbitals by using *occupancy-weighted symmetry orthogonalization*. This is an eigen decomposition akin to the Löwdin transformation³⁷ but on atomic angular symmetry blocks in the density matrix and is weighted by orbital occupancy. To describe the atomic state in a molecule, the Rydberg states (i.e., the unoccupied orbitals in the free ground-state atom) are allowed to become

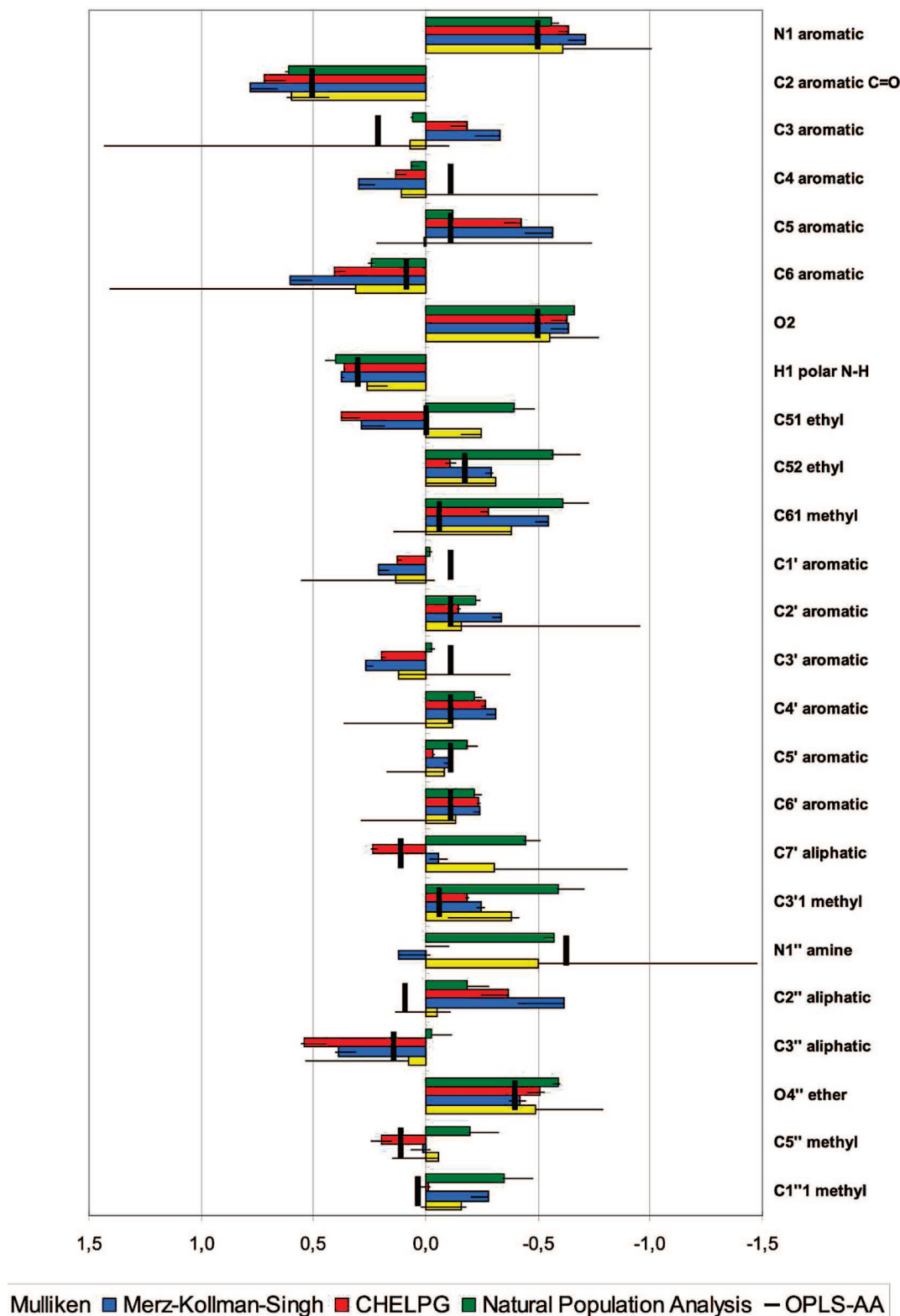


Figure 3. Calculated *ab initio* partial charges for compound **62** from Mulliken, Merz–Kollman-Singh, CHELPG, and Natural Population Analysis, compared to the OPLS-AA fragment charges. Charges derived from the most accurate description of the wave function, i.e. B3LYP/6–311+G(d,p) are shown in colored bars, except for the Mulliken charges where instead the B3LYP/6–31G(d,p) level is shown. The span between the maximum and minimum charges for the different basis sets, i.e. 6–31G(d,p), 6–31+G(d,p), 6–311G(d,p), and 6–311+G(d,p), are given by the error bars. The atomic numbering corresponds to that shown in Figure 2.

weakly populated. The populations are then given by the eigenvalues in this decomposition.

In Atoms in Molecules theory (AIM) by Bader^{17,18} the nuclei of the molecule are attractors of the gradient density field, and an atom is consequently defined as being the basin

containing all the gradient trajectories terminating in its nucleus. Integrating the density over this basin then gives the atomic populations.

In lieu of populations, one may fit monopole charges to the overall molecular electrostatic potential (ESP). Originally

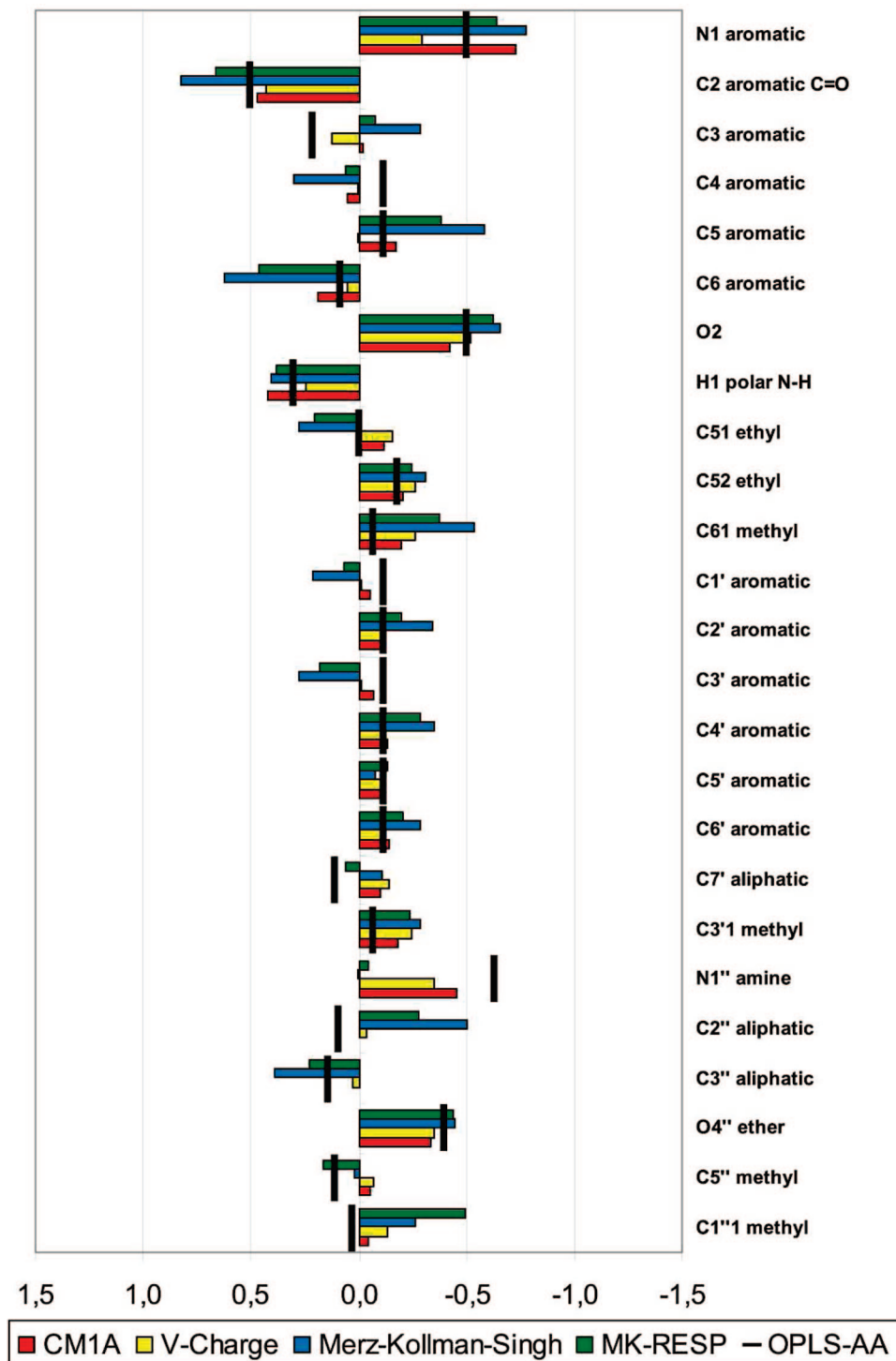


Figure 4. Calculated RESP, MK and semiempirical partial charges for compound **62**. The MK charges are identical to the ones in Figure 3 and were added for comparison with RESP. The atomic numbering corresponds to that shown in Figure 2.

introduced by Momany³⁸ and Cox and Williams,³⁹ these methods are based on the total density, which is a quantum mechanical observable, and will thus provide experimentally verifiable dipole and higher order multipole moments. In the Merz–Kollman–Singh (MK) variant, the potential is evaluated at points placed on the Connolly surface of the molecule^{40,41} onto which the charges are fitted in a least-squares manner, with a total integer charge constraint by the method of Lagrange multipliers.^{20,42} The Charges from Electrostatic Potentials scheme (CHELP) by Chirlian and

Franci⁴³ is similar but with the points placed in concentric, symmetric, and nearly spherical shells about the atoms. Breneman and Wiberg¹⁹ suggested that the potential instead be evaluated in a grid of uniformly spaced points (CHELPG) to dampen its sensitivity toward conformational changes and is the variant that is used here.

Being evaluated at some distance (about 1.5–2.0 times the van der Waals-radii²⁰), the charges of buried atoms (e.g., sp^3 carbons) have a tendency of being less important for the quality of the ESP fit than atoms closer to the molecular

Table 2. Static Average Polarizabilities and Dipole Moments in Gaseous and Aqueous Phase for the Compounds Studied Here, Using Two Levels of Theory

	B3LYP/6-31G(d,p)				B3LYP/6-311+G(d,p)			
	α [a_0^3]	$\mu(g)$ [D]	$\mu(aq)$ [D]	$\Delta\mu$	$\mu(g)$ [D]	$\mu(aq)$ [D]	$\Delta\mu$	
39	243	4.08	5.65	1.57	4.44	6.35	1.91	
40	259	3.84	5.26	1.42	4.03	5.65	1.62	
41	270	5.97	7.78	1.81	6.32	8.48	2.16	
46	244	4.02	5.86	1.84	4.36	6.64	2.28	
49	248	3.38	4.84	1.46	3.78	5.68	1.90	
52	273	4.23	5.69	1.46	4.68	6.54	1.87	
60	234	5.02	6.71	1.69	5.37	7.39	2.02	
62	233	4.81	6.71	1.89	5.29	7.65	2.36	
65	228	2.26	2.70	0.44	2.40	2.95	0.54	
68	294	5.56	8.40	2.84	5.76	9.07	3.31	

surface. For this reason, Bayly et al.⁴⁴ suggested that the charges on enveloped atoms be restrained with penalty functions to dampen arbitrary fluctuations and to enforce symmetry invariance, without deteriorating the overall description of the potential. Termed the Restrained Electrostatic Potential (RESP) method this procedure is used in the AMBER force field definition.^{45,46}

To reduce the computational effort, Cramer, Truhlar, and co-workers introduced the Charge Model 1A (CM1A) which extracts Mulliken populations from NNDO Austin Model 1 (AM1)⁴⁷ semiempirical wave functions and subsequently maps them with a multilinear form to reproduce experimentally observed dipole moments.²¹ These charges have been successfully used in solvation free energy calculations with the OPLS-AA force field.^{13,48,49}

Charges can also be inferred from the concept of electronegativity equalization where the atomic electron densities are shifted to atoms with higher electronegativity upon bond formation, thus giving rise to partial charges. The subsequent increase in atomic radius corresponds to a lowering in electronegativity which continues until equilibrium has been reached. Since total equalization will result in e.g. all atoms in a molecule of the same sort having identical charges, Gasteiger and Marsili suggested a partial equalization based on orbital electronegativities⁵⁰ where the charge transfer is somewhat dampened.⁵¹ In the Vcharge method, which is used here, Gilson et al. instead adjusted the initial electronegativities based on the properties of neighboring atoms, valence bond types, and a set of variables. The variables were parametrized on a set of compounds to reproduce the *ab initio* molecular ESP from the Hartree-Fock/6-31G(d) model chemistry.²² These methods are computationally cheap and only require the chemical structure formula of the molecule.

Finally, charges have been derived in analogy with the OPLS-AA force field definition,²⁹ where e.g. charges of the toluene molecule is found by maintaining the symmetric benzene charges and then adjusting the methyl carbon charges to maintain the overall charge group neutrality, as shown in Figure 1. Such charges are henceforth referred to as the OPLS-AA fragment based charges. Although charge redistribution between fragments is not taken into account, these charges are most likely to remain balanced with the force field parameters of the water model and the protein.

It may be noted that the Maestro software from Schrödinger uses an automated fragment-based method with bond charge increments⁵² to estimate junction atom charges. However, since this method requires optimized parameters for it to be applicable to the OPLS-AA force field and they are not publically available, this method will not be covered in the present work.

The *ab initio* Mulliken, MK, CHELPG, and NPA charges were derived from density functional theory (DFT) wave functions at two levels of theory on structures optimized in the gas phase—namely B3LYP/6-31G(d,p)//B3LYP/6-31(d,p) and B3LYP/6-31G(d,p)//B3LYP/6-311+G(d,p). That is, using the Becke three parameter hybrid functional⁵³ and the correlation functional of Lee, Yang, and Parr (B3LYP),^{54,55} together with Pople's polarized split valence and triple split contracted Gaussian basis sets, augmented with diffuse functions in the latter case.⁵⁶ Furthermore, to get an estimate of the basis set dependence of the different charge schemes, wave functions were formed using the additional basis sets 6-31+G(d,p) and 6-311G(d,p) for compound **62**, from which populations were derived with the methods outlined above. Where nothing else is stated the Gaussian 03 package⁵⁷ was used for all *ab initio* calculations.

The AIM calculations were performed with Bader's original AIMPAC source code, using the PROMEGA algorithm bundled in PROAIMV.⁵⁸ However, since the original settings only support molecules of at most 50 atoms, and the ligands considered herein are somewhat larger, the MCENT parameter was increased throughout the source code to allow a maximum of 60 centers instead. The adopted numerical integration parameters in the PROMEGA algorithm were 64 phi planes, 48 theta planes, and 96 radial points per integration ray within the Beta sphere. These settings yielded an underestimation of the atomic basin populations in the order of 3 to 6 $\cdot 10^{-4} e$. To correct for these artificial positive charges, the overall deviation from neutrality was divided equally across all basins and were subsequently subtracted. Although the absolute atomic net charges were affected by this correction, their relative charge differences were preserved.

To comply with the recommendations regarding the RESP calculation scheme,⁴⁴ Hartree-Fock densities with the 6-31G(d) basis set were also formed from which the MK ESP was extracted. RESP fitting of these charges were performed in two steps with the antechamber utility from the AmberTools distribution,^{59,60} using the ESP explicit output Gaussian internal option (IOP) 6/33=2. The ESP evaluation was set to 6 points per unit area using the IOP 6/42=6.

CM1A charges were calculated with the Amsol software,⁶¹ and Gilson charges were obtained with Vcharge⁶² (VC/2004 parameter set). As mentioned above, partial charges for the OPLS-AA charge set were assigned in analogy with the force field, except for the amine substituent of compound **68** where RESP charges were used.

Charge Polarization. The propensity of a compound to become polarized when exposed to surroundings can be gauged by calculating its static polarizability tensor α . This

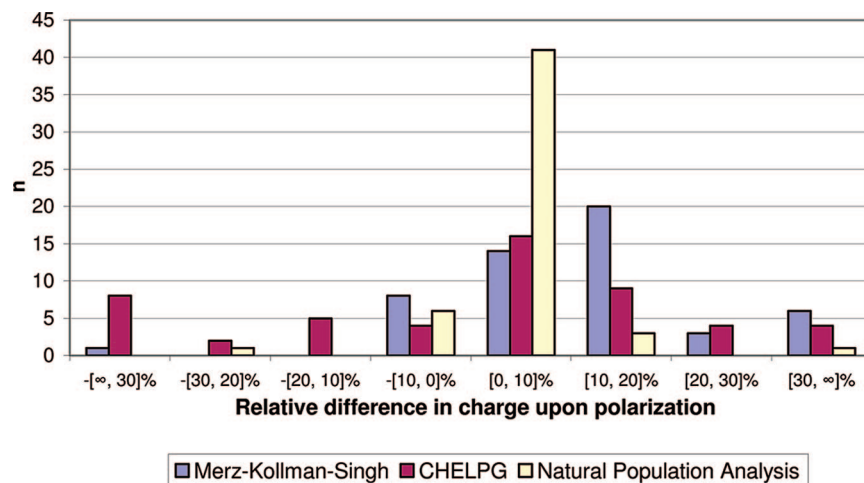


Figure 5. The impact of continuum solvent polarization on ESP charges (Merz–Kollman–Singh and CHELPG) as well as Natural Population Analysis for compound **62**. The histogram shows the number of atoms in this compound that have adjusted their charge within a certain range when exposed to the continuum solvent (e.g., for NPA, 41 out of 52 atoms have adjusted their partial charge by less than 10%).

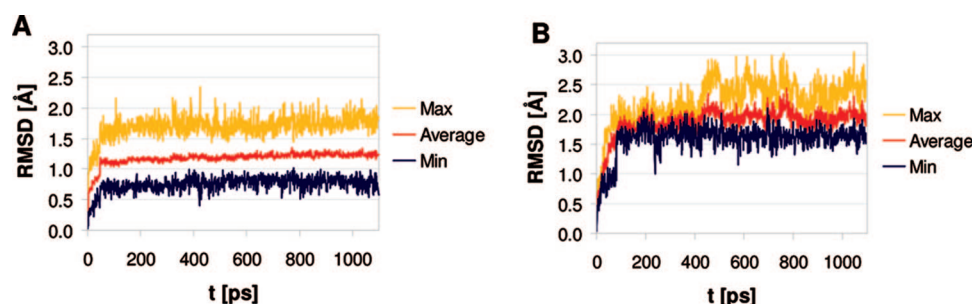


Figure 6. Extremum and average RMSD values across protein equilibration and production runs with the OPLS-AA fragment based charges are shown in panel A, with the exception of the ligand **52** runs which are shown separately in panel B. The RMSD scales in these plots have been kept equal for comparison.

tensor as well as higher order hyperpolarizabilities can be obtained from *ab initio* calculations where they are identified with the analytic derivatives of the energy with respect to the electric field at vanishing field strength.⁶³ Furthermore, the average polarizability $\bar{\alpha}$, i.e. the mean of the tensor diagonal elements, is an invariant that can be inferred from experiments.⁶⁴

Solvent induced polarization of the wave function can be modeled using Self Consistent Reaction Field theory (SCRF) where the solute molecule is placed in a cavity submersed in an infinite continuous polarizable medium. To this end, a conductor-like extension of Tomasi's apparent charge Polarizable Continuum Model^{65,66} (PCM), similar to the COSMO method by Klamt and Schüürman^{67,68} and termed Conductor-like PCM^{23,69} (CPCM), was used here.

Polarizabilities were extracted from frequency calculations at the B3LYP/6–31G(d,p) level of theory. Where imaginary frequencies were detected, or the magnitude of the rotational low frequencies surpassed $\sim 10 \text{ cm}^{-1}$, the optimizations were resubmitted with increased accuracy in the integration grid (see e.g. ref 70). The pruned UltraFine grid, with its 99 radial shells and 590 angular points, proved to be sufficient in all such cases.

CPCM polarization was implemented with the Gaussian keyword, using the standard permittivity for water and the

default number of tesserae per sphere. Furthermore, the atomic radii of the United Atom Kohn–Sham topological model (UAKS) were used in all B3LYP calculations since these radii have been optimized with respect to DFT using the parameter free Perdew, Burke, and Ernzerhof functional (PBE0) at the 6–31G(d) level of theory.⁵⁷ However, in the RESP Hartree–Fock calculations the default UA0 radii were used.

Statistical Measures. The accuracy of the LIE binding free energy estimates with the different partial charge sets was measured with the coefficient of determination, denoted R^2 . Since the coefficient of determination compares the variance of the predictions with the total variance in the data, it is commonly used to measure the extent to which the model explains the observed variance. For these purposes, however, it is enough to regard R^2 as a simple indication of the goodness-of-fit of the experimental data to the LIE regression line. Appropriately, the LIE parameters that have been optimized here, e.g. the γ parameter in the LIE standard model, have been done so by least-squares regression, i.e. by minimizing the *SSE* with respect to experimental data.

Apart from gauging the extent of explained variance in the model, it is also of special interest to measure the degree of correspondence between the rankings, or the *rank cor-*

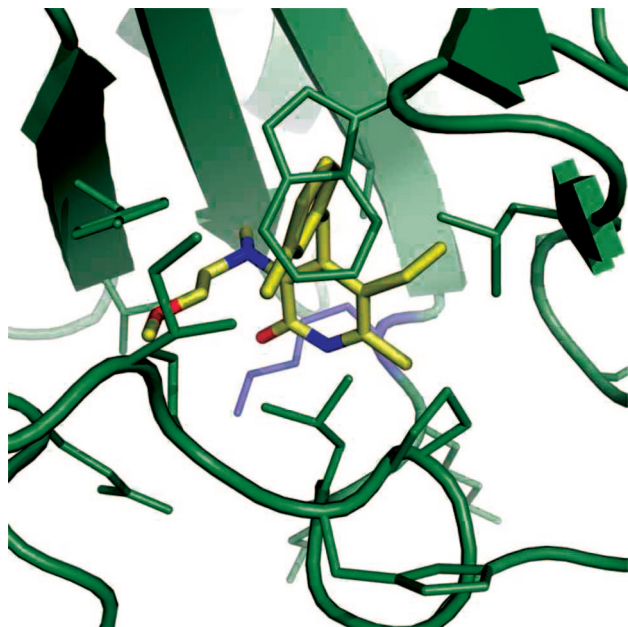


Figure 7. HIV-1 RT (green) in complex with compound **62** (yellow). The structure is a docking solution used as a starting structure in MD simulations. The figure shows the close proximity of Lys103 (blue) to the carbonyl oxygen of the pyridine.

relation,⁷¹ between the observed and calculated binding free energies. A popular way of doing this in virtual high-throughput screening⁷² is by computing Spearman's ρ value, given by

$$\rho = 1 - \frac{6S(d^2)}{n^3 - n} \quad (3)$$

where n is the number of observations, and $S(d^2)$ denotes the sum of squared differences between the experimental and calculated ranking for each observation. Spearman's ρ will thus be +1 if there is perfect agreement between the rankings, -1 if the sets are anticorrelated, and 0 if there is no agreement at all.

The error of the calculated binding free energy was estimated with the standard error of the mean (SEM) taken with respect to the ensemble averages in the protein starting from the three docking poses of each ligand. Given that the sample based estimation of the standard deviation is s and the number of observations is n —in this case three—the error then reads

$$\text{Err}[\Delta G_{\text{calc}}] = \alpha \frac{s[\langle U_{\text{lig-surr}}^{\text{vdw}} \rangle_{\text{prot}}]}{\sqrt{n}} + \beta \frac{s[\langle U_{\text{lig-surr}}^{\text{el}} \rangle_{\text{prot}}]}{\sqrt{n}}$$

Here it is assumed that the α and β parameters do not contribute significantly to the uncertainty of the estimation when the LIE standard model is used.

Furthermore, leave-one-out cross-validated R^2 , commonly referred to as Q_{Loo}^2 , has been used as a quantitative method to assess the predictive ability of the different LIE models and charge sets presented here. The definition of Q_{Loo}^2 is similar to that of R^2 , namely

$$Q_{\text{Loo}}^2 = 1 - \frac{\sum_i (\Delta G_i^{\text{obs}} - \Delta G_i^{\text{calc}})^2}{\sum_i (\Delta G_i^{\text{obs}} - \overline{\Delta G})^2} \quad (4)$$

The difference is that the binding energy of the i th ligand is estimated with a regression model on a data set where that particular compound was left out. If the model is dependent on the data points from which it was derived, this will have an impact on the Q_{Loo}^2 value. Following common practice, charge sets that fall short of producing a $Q_{\text{Loo}}^2 \geq 0.5$ will be ruled out. Although external validation is the most reliable method to assess predictability,⁷³ internal validation is deemed quite adequate for these purposes. However, Q^2 can give a slight underestimation of the true predictive error when applied to small data sets.⁷⁴

Structural Stability and Convergence. The structural stability of the ligand-protein complexes was estimated with the root-mean-square deviation (RMSD), given as

$$\text{RMSD}([\vec{u}_1 \dots \vec{u}_n], [\vec{v}_1 \dots \vec{v}_n]) = \sqrt{\frac{1}{n} \sum_{i=1}^n (\vec{u}_i - \vec{v}_i)^2} \quad (5)$$

In this case the RMSD was taken with respect to the heavy atom position vectors of the ligand structures, which were kept unfitted since the ligands are more or less held in position by the protein. By this choice rotation and translation are expected to have a significant impact on the computed values.

Before considering the impact of varying charges, the structural stability of the OPLS-AA fragment based charge runs was measured with respect to the starting structures, $[\vec{x}(0)_{1\dots n}]_i^j$, of ligand i and pose j , hence $\text{RMSD}(t) - ([\vec{x}(0)_{1\dots n}]_i^j, [\vec{x}(t)_{1\dots n}]_i^j)$. Then the charge model (CM) stability was measured by forming production phase average structures, $\langle \text{CM} \rangle$, and computing their RMSD with respect to OPLS-AA. That is, for the n th charge model this reads $\text{RMSD}(\langle \text{OPLSAA} \rangle_i^j, \langle \text{CM}_n \rangle_i^j)$, for ligand i and pose j . The former comparison is meant to gauge the overall stability of the system *per se*, whereas the latter reflects the impact of charge variation on the structures.

Since the RMSD values were extracted from 690 MD runs, a few operations were defined to simplify the presentation of this data. For the initial OPLS-AA stability, extremum and average RMSD values across all ligands and poses as a function of time are presented. When comparing charge models with the OPLS-AA average structures, the RMSD values were summed over the poses, that is $\sum_j \text{RMSD}(\langle \text{OPLSAA} \rangle_i^j, \langle \text{CM}_n \rangle_i^j)$.

Results and Discussion

To begin with, the actual differences in charge between the models will be investigated for a representative compound from the ligand set. Then the calculated polarizabilities and their impact on the calculated effective dipole moments, i.e. when subjected to implicit solvent, are presented. After this, the charge sets are culled, first with respect to the precision, as given by the convergence of the MD ensemble averages,

and then on the accuracy in their binding free energy estimates. Finally, the reliability of these results is examined through statistical internal validation.

Comparing Charges. To get an overview of how partial charges actually differ between the charge models, ligand **62** (see Figure 2) was chosen as a representative compound, and the derived *ab initio* charges of its first row atoms and the polar N–H hydrogen are displayed in Figure 3. To begin with, charge dependence on level of the model chemistry was gauged by performing DFT calculations with a range of basis sets, namely 6–31G(d,p) and 6–311G(d,p) with and without the addition of diffuse functions. Charges derived from the highest level of theory are displayed in Figure 3, with the exception of the Mulliken charges where instead the low level is shown, as well as the span between the charge assignments which is shown in the error bars. As expected, the sensitivity toward the choice of basis set is most apparent for the Mulliken charges, where for instance the C3 atom of the pyridinone ring (defined in Figure 2) ranges from being neutral to highly negative (~ -1.5 e) when adding diffuse functions. This is presumably due to the considerable overlap populations. In contrast, the NPA and the ESP charges are significantly more stable in this respect.

Apart from basis set impact, charge assignment from the different methods is seen to vary throughout, which is only natural considering that the atomic partial charges are not quantum mechanical observables and thus cannot be directly measured by experiment. Any charge assignment will therefore be more or less arbitrary. In particular, substituent atoms that link functional groups together seem to be difficult to assign by any method, e.g. C51, C7', the tertiary N1'', and its neighbors. However, there are a few cases where there is a remarkable agreement between all the methods, such as the ether O4'' and the pyridinone polar H1 atoms. Also, it is reassuring to see an overall similarity between the ESP charges from the MK and CHELPG schemes. Moreover, charge redistribution seems to be causing the most pronounced overall difference between the OPLS-AA fragment based charges and the *ab initio* sets. For instance, the aromatic C1'–C6' atoms are seen to be in fair agreement except where the aliphatic substituents are bound, i.e. C1' and C3'. This can also be seen in the pyridinone ring C3 and C4 atoms.

In order to compare the CM1A and Vcharge sets with OPLS-AA and *ab initio* charges, they are plotted along with the MK ESP charges in Figure 4. Also included in this plot are the RESP fitted charges, which were extracted from the Hartree–Fock ESP using the 6–31G(d) basis set, rather than the high level DFT wave functions. In spite of these differences, the RESP charges are seen to be very similar to the MK set.

The overall picture that emerges in this figure is just about the same as in Figure 3. The charge redistribution that is disregarded in the fragment based method is indeed captured by the empirical models, where CM1A seems to lie closest to the OPLS-AA charges. The overall RMSD between the CM1A and Vcharge set is 0.09 e, the largest difference being the pyridinone nitrogen where CM1A is substantially more polarized. There are a few cases where they deviate from

OPLS-AA, e.g. the amine N1'' and C7', but the impression is that they are more consistent with the force field than the MK and RESP charges.

Polarizability and Solvent Effects. The charges that were discussed in the previous section were all derived *in vacuo*. However, drug binding and hydration pertain to polar surroundings that can have a significant impact on the overall electrostatic properties of the compound due to polarization. For this reason, it seems useful to estimate the importance of charge polarization for these compounds, either by including an environment in the calculation or by studying their intrinsic static average polarizability in vacuum. In the latter case, a significant polarizability indicates that the charges may vary as the ligand is subjected to different surroundings. The polarizability of the wave function was thus calculated and compared with the change in dipole moment as the compounds are subjected to the implicit solvation model. As expected, the presence of aromatic groups results in significant polarizabilities ranging from about 200 to 300 a_0^3 (see Table 2), which may be compared with the polarizability of, for instance, water which is 10.13 a_0^3 ($\Delta_{\text{calc-exp}} = -4.78$ a_0^3), methane 16.52 ($\Delta_{\text{calc-exp}} = -3.84$) a_0^3 , and ammonia 14.19 ($\Delta_{\text{calc-exp}} = -5.61$) a_0^3 , with the model chemistry used here (values from ref 75), where a_0 is the Bohr radius. This is in turn reflected in the significant increase of the dipole moment, by up to 3 D, when exposed to the implicit solvent model (see Table 2).

It seems rather clear that the impact of the solvent on the total charge distribution, as represented by the dipole moments, should also appear as changes in the partial charges. Indeed, plotting the distributions of the relative changes in atomic charge when compound **62** is exposed to solvent shows that they change by 10% or more due to polarization when ESP methods are used (see Figure 5). In contrast, polarization does not seem to affect NPA charges as much, where only four atoms change by more than 10%. This difference can perhaps be understood by considering that the ESP is directly based on the overall charge distribution. The increase in the dipole moments and its impact on the partial charges substantiates the typical choice of using charges derived from the HF/6–31G(d) level of theory,⁴⁴ which usually overestimates the dipole moment of the molecule to an extent that roughly corresponds to its effective value in aqueous solution. However, it should be noted that this effect does not seem to be as pronounced for the B3LYP model chemistries that are used here.⁷⁵ Charge polarization is also the motivation behind linear scaling of charges present in the OPLS/CM1A force field,⁴⁸ i.e. where the CM1A charges are multiplied by a factor of 1.14 to enhance solvation free energy estimates. This linear scaling has also been included in this study.

Stability and Convergence. As outlined in the Methods section, the binding free energy estimates in the LIE method are calculated from ensemble averages of the ligand-surrounding interaction energies, which are extracted from molecular dynamics trajectories. Every ligand is simulated from three different docking poses for every charge set, and

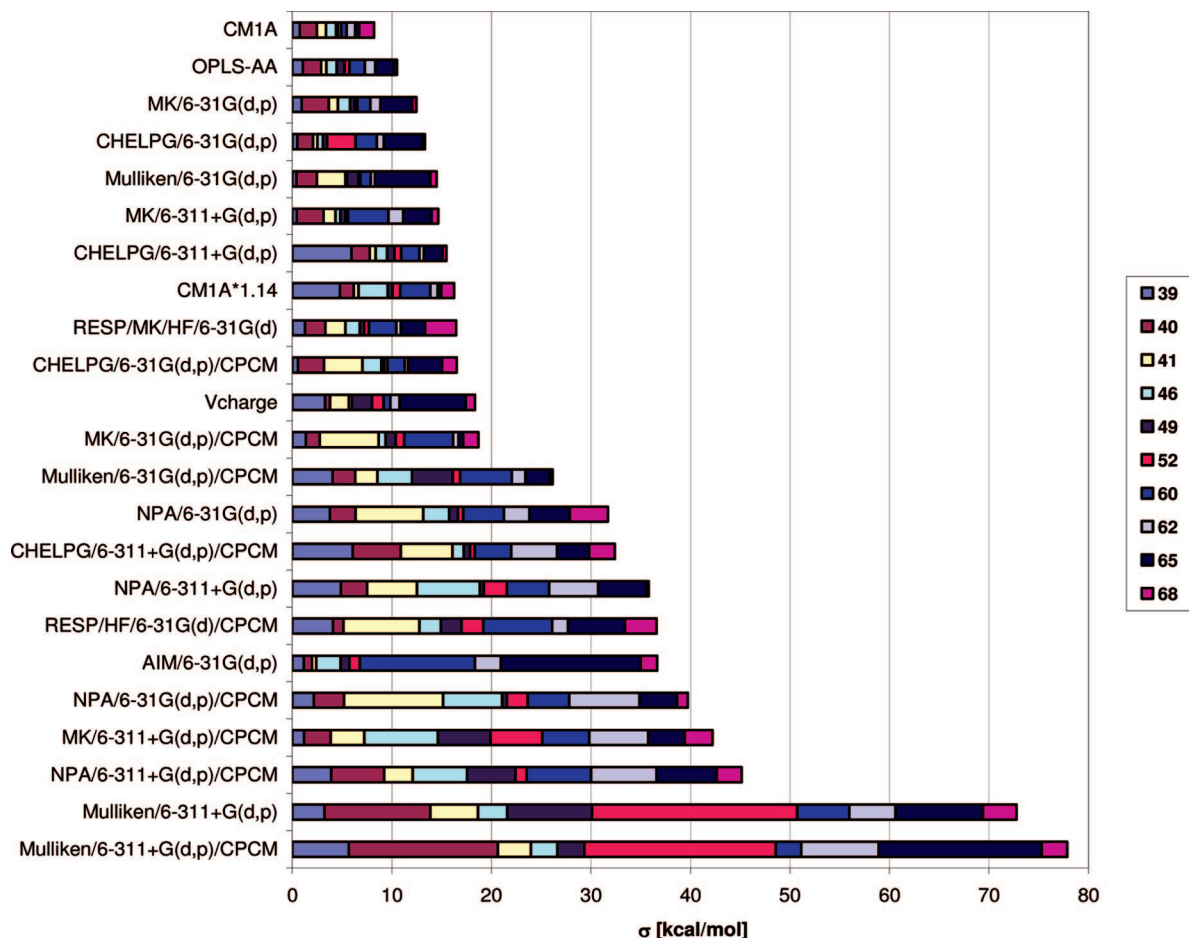


Figure 8. Standard deviations of the triplicate $\langle U_{i,s}^{\text{el}} \rangle$ protein–ligand electrostatic energies for each ligand, accumulated for each charge set.

since these poses were selected from the same binding mode the resulting energies are given as the mean from the three simulations. It should be noted that in cases where poses cannot interchange during the course of the simulation it would be hard to justify that they are in thermal equilibrium and so the averages would have to be Boltzmann weighted.

It is important that the MD runs have converged structurally and energetically, both within one and the same run and between simulations with different docking poses, since this will determine the precision in the binding free energy estimates. Structurally, the simulations are stable with low RMSD of the ligands and only minor fluctuations in the protein. Specifically, in the reference OPLS-AA charge simulations the maximum unfitted RMSD among the ten inhibitors and their three poses is largest for compound **52**, namely 3.1 Å, whereas it does not exceed 2.3 Å for the other ligands. However, the largest contribution to this value occurs during equilibration, after which the ligands have settled into a position on average differing by 1.9 Å for compound **52** and 1.2 Å for the rest (Figure 6). After this initial displacement the fluctuations about their equilibrated positions are quite small. Such small variations are expected since the inhibitors are rigid and bind to a well-defined allosteric pocket. The main structural fluctuation, occurring only in a few cases, is found in the side chain of Lys103, which is located close to the carbonyl group of the pyridinone ring in the docked starting position (Figure 7) as well as in the

crystal structure.²⁶ In cases where this lysine leaves the carboxyl group and starts to interact with the solvent, the electrostatic ligand-surrounding energies are substantially decreased, which results in an increase in the predicted binding free energy.

Turning to the energies, convergence within runs is easily examined and is seen to be satisfactory in all cases. However, convergence between docking poses requires some additional figure of measure. To this end, the standard deviation of the protein–ligand electrostatic interaction energy between triplicates has been adopted, since it is the electrostatic energy that gives the largest contribution to the error and is mostly affected upon exchange of partial charges. Indeed, the van der Waals interaction energies were seen to be fairly constant throughout the simulations. As shown in Figure 8, the cumulative standard deviations of the ligand-protein electrostatic interaction energies span an order of magnitude, where CM1A and the standard OPLS-AA charge sets give the most converged estimations. Interestingly, CM1A charges are seen to give better convergence in this respect than the OPLS-AA fragment based method. On the other hand, charge polarization either by linear scaling or continuum solvent consistently increases the binding free energy error. As expected, Mulliken populations with diffuse basis sets stand out as a terrible choice by this measure.

At this point it is important to remember that precision by itself has little or no merit if the accuracy of the

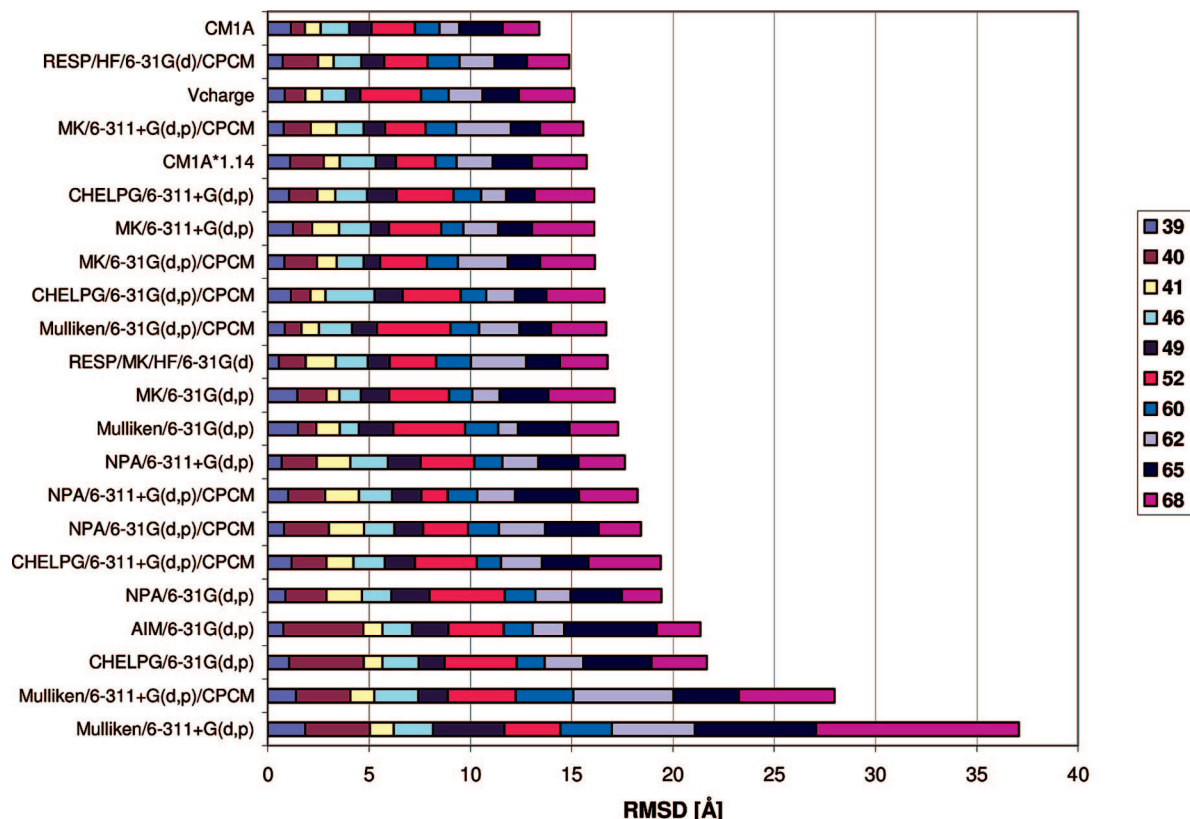


Figure 9. RMSD values between average structures of the OPLS-AA and the different charge model simulations summed over poses, that is $\sum_i \text{RMSD}(\langle \text{OPLSAA} \rangle_i, \langle \text{CM}_n \rangle_i)$, accumulated for each charge model.

predictions is disregarded. For instance, with the present figure of measure one would obtain a very high precision by neutralizing all the charges but at a cost of severely reducing the accuracy of the predictions. Conversely, if there are models here that give highly accurate predictions but with a very low precision, they will be hard to distinguish from random noise—especially on such a limited number of observations. For this reason, it is argued that both precision and accuracy are of moment here, and charge sets with an accumulated standard deviation in ligand-surrounding electrostatic energies that exceeds 20 kcal/mol are therefore discarded henceforth.

Since there are considerable variations in the electrostatic ligand-surrounding energies, one may question whether this is reflected in the structural stability of the bound complex. As judged by the $\sum_i \text{RMSD}(\langle \text{OPLSAA} \rangle_i, \langle \text{CM}_n \rangle_i)$ values shown in Figures 9 and 10 however, the structures seem not to be greatly affected by the choice of charges, except for the aforementioned rather extreme Mulliken populations. One may also note that the CHELPG/6-31G(d,p) model, with a rather large accumulated RMSD in Figure 9, still is among the most precise models with respect to ligand-surrounding electrostatic energies in Figure 8. Hence, the precision in the binding free energy estimation does not appear very sensitive to minor structural rearrangements of the ligand-protein complexes. Furthermore, from Figure 10 it seems that the structural variations are inherent to the ligand rather than the charge model. Indeed, plotting the most aberrant average structure in this respect, namely compound **68** with the Mulliken/6-311+G(d,p) charge set, together with the OPLS-AA average structure and its corresponding initial

docking pose, reveals that the significant unfitted RMSD in this case is due to translation and rotation of the ligand and not a change in the actual binding mode (see Figure 11).

Relative Binding Free Energies. After optimization of the constant offset parameter γ in the LIE standard model, the accuracy of the calculated relative binding free energies from the different charge sets was estimated through the coefficient of determination (R^2), Spearman's coefficient of rank correlation (ρ), and the mean unsigned error ($\langle |Err| \rangle$) with respect to experimental data. The results are given in descending order of accuracy with respect to R^2 in Table 3 together with the rms difference in charge from the OPLS-AA fragment method. *Caveat lector*—as already mentioned the compounds were selected from our previous study²⁴ to give accurate binding free energies and to be well behaved during simulations with the OPLS-AA force field. However, since the R^2 for all the compounds in the original study was 0.70 and the ten compounds selected here score better than average with an R^2 of 0.90 (see Figure 12A), there is a slight statistical bias toward these charges. In the same way, the unsigned average error was 0.80 kcal/mol in the original data set, whereas it is 0.49 kcal/mol for this subset. This is not a major concern however, since our aim is rather to compare the remainder of the methods with respect to each other than with respect to the fragment based method. The performance of this method in binding free energy calculations is already known (see for instance the original data set²⁴).

Bearing this in mind, MK ESP charges from the B3LYP/6-311+G(d,p) model chemistry emerge with the highest recorded accuracy with respect to R^2 , shown in Figure 12B,

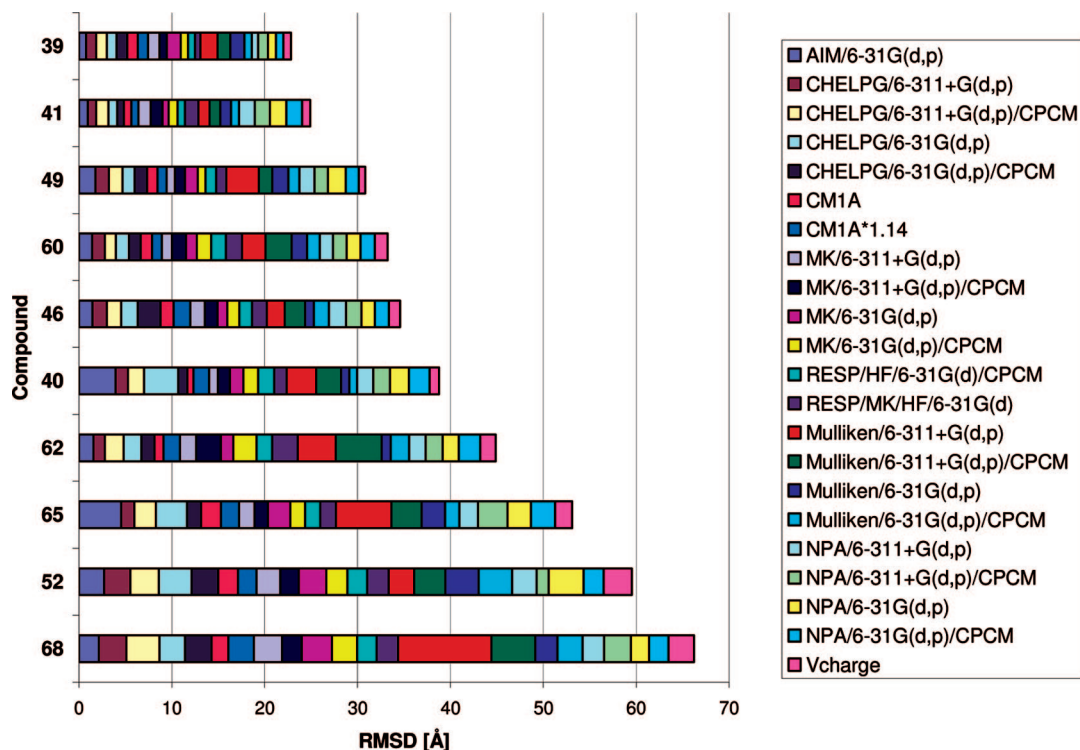


Figure 10. RMSD values between average structures of the OPLS-AA and the different charge model simulations summed over poses, that is $\sum_j \text{RMSD}(\langle \text{OPLSAA} \rangle_j, \langle \text{CM}_n \rangle_j)$, accumulated for each ligand.

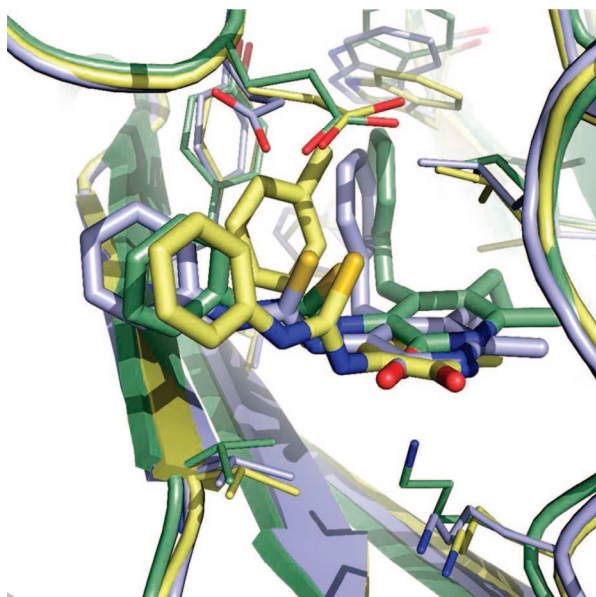


Figure 11. The docked pose for compound **68** in green, superpositioned with the corresponding OPLS-AA and Mulliken/6-311+G(d,p) average structures in blue and yellow, respectively. The Mulliken average structure is the most disparate with respect to OPLS-AA in terms of RMSD.

closely followed by CM1A and Vcharge in Figure 12C,D. However, taking the mean unsigned error into account the ESP method is superseded by CM1A, which is mainly due to the outlying compound **46** whose squared residual inflicts a heavy penalty on the coefficient of determination, as can be seen in Figure 13. From Figure 12 it seems fairly clear that the two bad binders **46** and **68**, whose experimental affinities are well separated from the rest, remain distin-

Table 3. Charge Deviations with Respect to the OPLS-AA Charges As Well as the Mean Unsigned Error, R^2 , Q^2 , and Spearman's ρ from Binding Free Energy Calculations for the Different Charge Sets^a

	charge RMSD ^b	$\langle \text{Err} \rangle$ ^c	R^2	Q^2	ρ	γ
OPLS-AA	N/A	0.49	0.90	0.88	0.96	-10.03
MK 6-311+G(d,p)	0.24	0.95	0.71	0.64	0.53	-8.97
CM1A	0.09	0.87	0.66	0.58	0.76	-10.35
Vcharge	0.09	1.09	0.64	0.56	0.61	-8.18
MK/6-31G(d,p)	0.20	1.11	0.61	0.52	0.67	-8.04
CHELPG/6-31G(d,p)	0.15	1.15	0.59	0.50	0.51	-7.48
Mulliken/6-31G(d,p)	0.14	1.20	0.53	0.42	0.61	-7.65
CM1A*1.14	0.10	1.34	0.40	0.26	0.70	-13.05
CHELPG/6-311+G(d,p)	0.18	1.41	0.36	0.21	0.35	-7.89
RESP/MK/HF 6-31G(d)	0.18	1.36	0.28	0.12	0.70	-8.93
MK/6-31G(d,p)/CPCM	0.21	1.56	-0.11	-0.37	0.67	-10.59
CHELPG/6-31G(d,p)/CPCM	0.16	1.90	-0.29	-0.59	0.44	-9.14

^a The methods are presented in descending order with respect to R^2 . ^b Given in [e]. ^c Given in [kcal/mol].

guished from the cluster of good binders for all these charge sets. However, Spearman's coefficient of rank correlation given in Table 3 seems to capture the apparent lack of agreement within the cluster of good binders for the MK/6-311+G(d,p) and CHELPG/6-31G(d,p) charges, giving a relatively low ρ of 0.53 and 0.51, respectively. This can be contrasted with the CM1A ranking where ρ is 0.76, followed by CM1A*1.14 and the RESP charges with a ρ of 0.70. Hence, the rather low values of R^2 and Q^2 for the latter two methods seem not to be reflected in the ranking of the compounds.

As judged from their relative contribution to the SSE in Figure 13, it appears that the compounds **46** and **62** are the hardest to predict with LIE regardless of charge model,

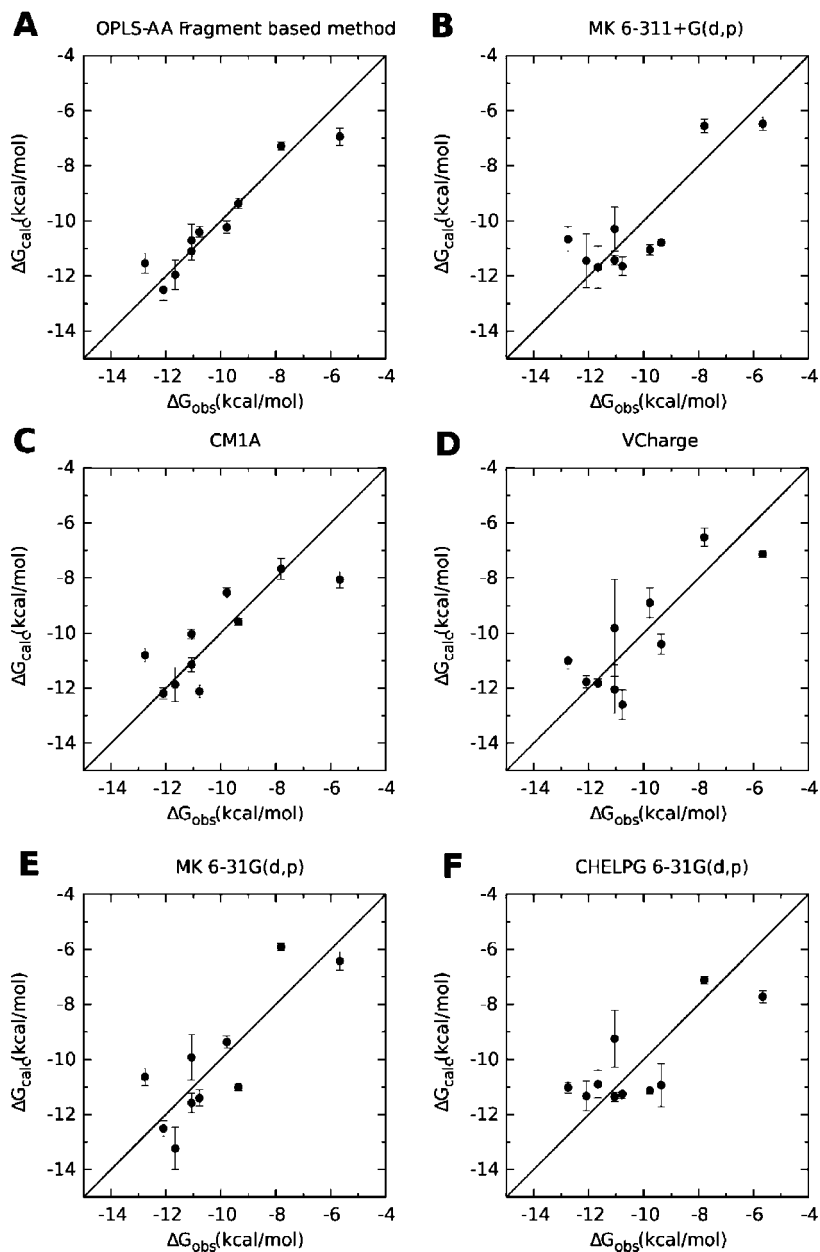


Figure 12. Calculated versus experimentally observed binding free energies for the highest ranked charge models in this survey.

whereas **52** and **68** have relatively inaccurate predictions with the ESP and Vcharge methods but not with CM1A and OPLS-AA. Ligands **52** and **68** have a benzyl group in the R_3 moiety in common, but the most striking differences in actual charge are rather found in the nonvariable part of the compounds.

Turning to the predictive ability, the six most accurate charge sets in Table 3 also have a $Q^2 \geq 0.5$ within the LIE standard model, which is considered acceptable for these purposes. Although leave-many-out cross-validation will generally provide a better measure of this, the two aforementioned bad binders would inflict a heavier penalty than warranted if two or more compounds were excluded in this process.

Interestingly, whereas CM1A and Vcharge produce sets that are relatively close to the OPLS-AA charges, as judged by the low charge rms of 0.09 e in Table 3, the MK ESP

charges are seen to differ with as much as 0.24 e . This could be compared with the least accurate scheme with respect to R^2 and the mean unsigned error given in this table, CHELPG from the solvent polarized B3LYP/6-31G(d,p) wave function, that has a significantly lower rms of 0.16 e but is seen to produce rather poor predictions. For this reason, the relative success of the MK ESP charges indicates that partial charges can still perform well with the LIE method even when they are dissimilar from the fragment based method charges, which are in turn derived to lie as close to the force field definition as possible. In contrast, the accuracy of CM1A and Vcharge presumably follows from their relative similarity with these charges.

Introducing solvent polarization, either by linear scaling or a continuum model, generally has a negative effect on accuracy both for the *ab initio* ESP schemes and CM1A. It is conceivable that these polarization models actually amplify

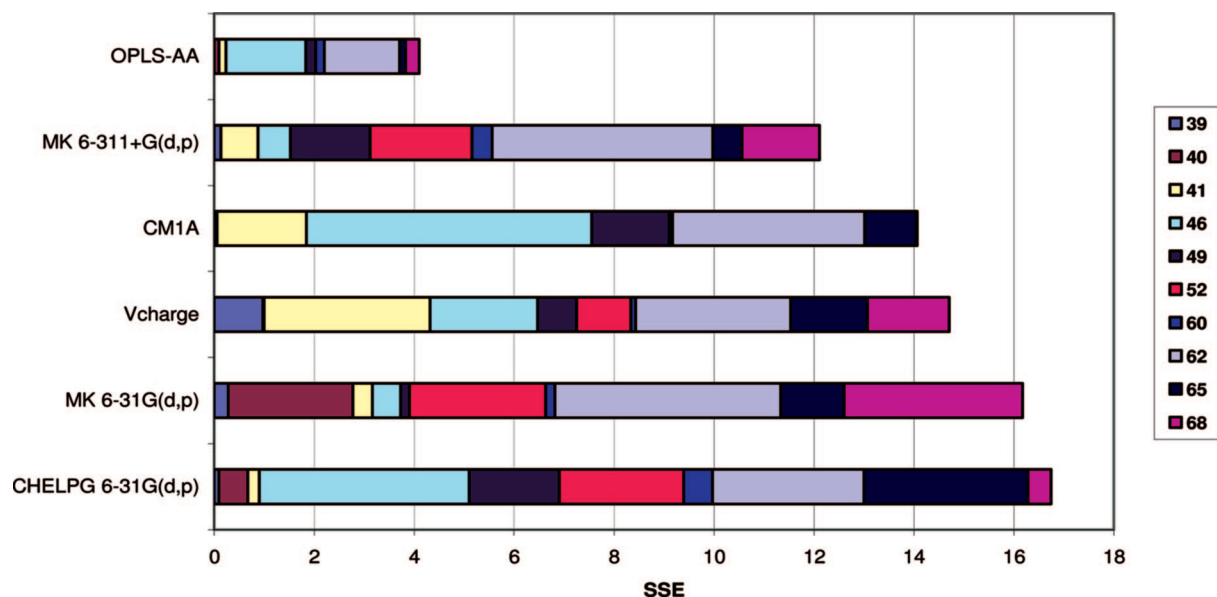


Figure 13. The contribution from each ligand to the sum of squared errors (SSE) with respect to experimental and calculated binding free energies for the highest ranked charge models.

errors in the charge assignment, such as the neglect of protein induced polarization. If this is the case, it is conceivable that ligand polarization by e.g. QM/MM methods⁷⁶ would provide better charge descriptions in this respect.

The fact that relatively minor changes in the rms charge when performing CM1A*1.14 linear scaling has a significantly negative impact on estimation accuracy may be somewhat unexpected, especially since it has been shown to give excellent hydration free energy estimates,^{13,14} but highlights the difference between solvation and binding free energies.

Taken together with the apparent success of ESP methods and simpler schemes adjusted to reproduce the overall electrostatic potential of the compounds, it appears that the LIE method is more sensitive toward observable changes in the electrostatic properties of the system than variations of the nonobservable and somewhat arbitrary partial charges of the constituent atoms. This suggests that these results should be readily transferrable to other protein systems and ligand classes as well. Furthermore, this could also be the reason why RESP fitting from the HF/6-31G(d) wave function is seen not to give nearly as precise predictions as the plain MK scheme applied to the higher level DFT density, although their charges are seen to be very similar (cf. Figure 4).

Conclusions

After having taken measures of precision, accuracy, and internal statistical validation into account, the Merz–Kollman–Singh, CM1A, Vcharge, and CHELPG schemes are seen to provide ligand partial charges that perform well in binding free energy calculations with LIE. Among these, CM1A and Vcharge are also both computationally cheap and easily automated. Since CM1A has the additional advantage of providing a good ranking correlation with respect to experiment, this method emerges as an attractive choice for high-throughput LIE with the OPLS-AA force field. In view of

the close relationship between LIE and free energy perturbation/thermodynamic integration simulations, one would expect that the results obtained herein also should apply to those methods.

Acknowledgment. We wish to thank Professor William Jorgensen for insightful comments on charge scaling. Support from the Swedish Foundation for Strategic Research (SSF/Rapid) and the Swedish Research Council (VR) is gratefully acknowledged.

References

- (1) Brandsdal, B. O.; Österberg, F.; Almlöf, M.; Feierberg, I.; Luzhkov, V. B.; Åqvist, J. *Adv. Protein Chem.* **2003**, *66*, 123–158.
- (2) Foloppe, N.; Hubbard, R. *Curr. Med. Chem.* **2006**, *13*, 3583–3608.
- (3) Gohlke, H.; Klebe, G. *Angew. Chem., Int. Ed.* **2002**, *41*, 2645–2676.
- (4) Åqvist, J.; Medina, C.; Samuelsson, J. E. *Protein Eng.* **1994**, *7*, 385–391.
- (5) Almlöf, M.; Brandsdal, B. O.; Åqvist, J. *J. Comput. Chem.* **2004**, *25*, 1242–1254.
- (6) Bjelic, S.; Nervall, M.; Gutierrez-de-Teran, H.; Ersmark, K.; Hallberg, A.; Åqvist, J. *Cell. Mol. Life Sci.* **2007**, *64*, 2285–2305.
- (7) Almlöf, M.; Andér, M.; Åqvist, J. *Biochemistry* **2007**, *46*, 200–209.
- (8) Andér, M.; Luzhkov, V. B.; Åqvist, J. *Biophys. J.* **2008**, *94*, 820–831.
- (9) Bortolato, A.; Moro, S. *J. Chem. Inf. Model.* **2007**, *47*, 572–582.
- (10) Carlsson, J.; Åqvist, J. *Phys. Chem. Chem. Phys.* **2006**, *8*, 5385–5395.
- (11) Huang, D. Z.; Luthi, U.; Kolb, P.; Cecchini, M.; Barberis, A.; Caffisch, A. *J. Am. Chem. Soc.* **2006**, *128*, 5436–5443.

- (12) Kolb, P.; Huang, D.; Dey, F.; Caflisch, A. *J. Med. Chem.* **2008**, *51*, 1179–1188.
- (13) Udier-Blagovic, M.; De Tirado, P. M.; Pearlman, S. A.; Jorgensen, W. L. *J. Comput. Chem.* **2004**, *25*, 1322–1332.
- (14) Mobley, D. L.; Dumont, E.; Chodera, J. D.; Dill, K. A. *J. Phys. Chem. B* **2007**, *111*, 2242–2254.
- (15) Mulliken, R. S. *J. Chem. Phys.* **1955**, *23*, 1833–1840.
- (16) Reed, A. E.; Weinstock, R. B.; Weinhold, F. *J. Chem. Phys.* **1985**, *83*, 735–746.
- (17) Bieglerkonig, F. W.; Bader, R. F. W.; Tang, T. H. *J. Comput. Chem.* **1982**, *3*, 317–328.
- (18) Bieglerkonig, F. W.; Nguyendang, T. T.; Tal, Y.; Bader, R. F. W.; Duke, A. J. *J. Phys. B: At., Mol. Opt. Phys.* **1981**, *14*, 2739–2751.
- (19) Breneman, C. M.; Wiberg, K. B. *J. Comput. Chem.* **1990**, *11*, 361–373.
- (20) Singh, U. C.; Kollman, P. A. *J. Comput. Chem.* **1984**, *5*, 129–145.
- (21) Storer, J. W.; Giesen, D. J.; Cramer, C. J.; Truhlar, D. G. *J. Comput.-Aided Mol. Des.* **1995**, *9*, 87–110.
- (22) Gilson, M. K.; Gilson, H. S. R.; Potter, M. J. *J. Chem. Inf. Comput. Sci.* **2003**, *43*, 1982–1997.
- (23) Barone, V.; Cossi, M. *J. Phys. Chem. A* **1998**, *102*, 1995–2001.
- (24) Carlsson, J.; Boukharta, L.; Åqvist, J. *J. Med. Chem.* **2008**, *51*, 2648–2656.
- (25) Benjahad, A.; Croisy, M.; Monneret, C.; Bisagni, E.; Mabire, D.; Coupa, S.; Poncelet, A.; Csoka, I.; Guillemont, J.; Meyer, C.; Andries, K.; Pauwels, R.; de Bethune, M. P.; Himmel, D. M.; Das, K.; Arnold, E.; Nguyen, C. H.; Grierson, D. S. *J. Med. Chem.* **2005**, *48*, 1948–1964.
- (26) Himmel, D. M.; Das, K.; Clark, A. D.; Hughes, S. H.; Benjahad, A.; Oumouch, S.; Guillemont, J.; Coupa, S.; Poncelet, A.; Csoka, I.; Meyer, C.; Andries, K.; Nguyen, C. H.; Grierson, D. S.; Arnold, E. *J. Med. Chem.* **2005**, *48*, 7582.
- (27) Jones, G.; Willett, P.; Glen, R. C.; Leach, A. R.; Taylor, R. *J. Mol. Biol.* **1997**, *267*, 727–748.
- (28) Marelus, J.; Kolmodin, K.; Feierberg, I.; Åqvist, J. *J. Mol. Graphics Modell.* **1998**, *16*, 213–225.
- (29) Jorgensen, W. L.; Maxwell, D. S.; TiradoRives, J. *J. Am. Chem. Soc.* **1996**, *118*, 11225–11236.
- (30) Jorgensen, W.; Chandrasekhar, J.; Madura, J.; Rw, I.; Klein, M. *J. Chem. Phys.* **1983**, *79*, 926–935.
- (31) Ryckaert, J. P.; Ciccotti, G.; Berendsen, H. J. C. *J. Comput. Phys.* **1977**, *23*, 327–341.
- (32) King, G.; Warshel, A. *J. Chem. Phys.* **1989**, *91*, 3647–3661.
- (33) Lee, F. S.; Warshel, A. *J. Chem. Phys.* **1992**, *97*, 3100–3107.
- (34) Åqvist, J.; Hansson, T. *J. Phys. Chem.* **1996**, *100*, 9512–9521.
- (35) Hansson, T.; Marelus, J.; Åqvist, J. *J. Comput.-Aided Mol. Des.* **1998**, *12*, 27–35.
- (36) Luthi, H. P.; Ammeter, J. H.; Almlof, J.; Faegri, K. *J. Chem. Phys.* **1982**, *77*, 2002–2009.
- (37) Löwdin, P. O. *J. Chem. Phys.* **1950**, *18*, 365–375.
- (38) Momany, F. A. *J. Phys. Chem.* **1978**, *82*, 592–601.
- (39) Cox, S. R.; Williams, D. E. *J. Comput. Chem.* **1981**, *2*, 304–323.
- (40) Connolly, M. L. *J. Appl. Crystallogr.* **1983**, *16*, 548–558.
- (41) Connolly, M. L. *Science* **1983**, *221*, 709–713.
- (42) Besler, B. H.; Merz, K. M.; Kollman, P. A. *J. Comput. Chem.* **1990**, *11*, 431–439.
- (43) Chirlian, L. E.; Francl, M. M. *J. Comput. Chem.* **1987**, *8*, 894–905.
- (44) Bayly, C. I.; Cieplak, P.; Cornell, W. D.; Kollman, P. A. *J. Phys. Chem.* **1993**, *97*, 10269–10280.
- (45) Cornell, W. D.; Cieplak, P.; Bayly, C. I.; Gould, I. R.; Merz, K. M.; Ferguson, D. M.; Spellmeyer, D. C.; Fox, T.; Caldwell, J. W.; Kollman, P. A. *J. Am. Chem. Soc.* **1996**, *118*, 2309–2309.
- (46) Wang, J. M.; Cieplak, P.; Kollman, P. A. *J. Comput. Chem.* **2000**, *21*, 1049–1074.
- (47) Dewar, M. J. S.; Zoebisch, E. G.; Healy, E. F.; Stewart, J. J. P. *J. Am. Chem. Soc.* **1985**, *107*, 3902–3909.
- (48) Jorgensen, W. L.; Tirado-Rives, J. *Proc. Natl. Acad. Sci. U.S.A.* **2005**, *102*, 6665–6670.
- (49) Kaminski, G. A.; Jorgensen, W. L. *J. Phys. Chem. B* **1998**, *102*, 1787–1796.
- (50) Hinze, J.; Whitehead, M. A.; Jaffe, H. H. *J. Am. Chem. Soc.* **1963**, *85*, 148.
- (51) Gasteiger, J.; Marsili, M. *Tetrahedron* **1980**, *36*, 3219–3228.
- (52) Halgren, T. A. *J. Comput. Chem.* **1996**, *17*, 616–641.
- (53) Becke, A. D. *J. Chem. Phys.* **1993**, *98*, 5648–5652.
- (54) Lee, C. T.; Yang, W. T.; Parr, R. G. *Phys. Rev. B* **1988**, *37*, 785–789.
- (55) Miehlisch, B.; Savin, A.; Stoll, H.; Preuss, H. *Chem. Phys. Lett.* **1989**, *157*, 200–206.
- (56) Frisch, M. J.; Pople, J. A.; Binkley, J. S. *J. Chem. Phys.* **1984**, *80*, 3265–3269.
- (57) *Gaussian 03, revision C.02*; Gaussian Inc.: Wallingford, CT, 2004.
- (58) *AIMPAC, version 94*; Department of Chemistry, McMaster University: Hamilton, Ontario, Canada, 1994.
- (59) *AmberTools, 1.2*; University of California: San Francisco, CA, 2008.
- (60) Case, D. A.; Cheatham, T. E., III; Darden, T.; Gohlke, H.; Luo, R.; Merz, K. M. J.; Onufriev, A.; Simmerling, C.; Wang, B.; Woods, R. J. *J. Comput. Chem.* **2005**, *26*, 1668.
- (61) *AMSO, version 7.0*; University of Minnesota: Minneapolis, MN, 2003.
- (62) *Vcharge, 1.0*; VeraChem LLC: Germantown, MD, 2004.
- (63) Pugh, D. Electric multipoles, polarizabilities and hyperpolarizabilities In *Chemical Modelling: Applications and Theory*; Hinchliffe, A., Ed.; RSC: Cambridge, U.K., 2000; Vol. 1, pp 1–37.
- (64) Herzberg G. Vibrational infrared and Raman spectra. In *Infrared and Raman spectra of polyatomic molecules*; 1st ed.; Van Nostrand: New York, NY 1945; pp 239–269.
- (65) Miertus, S.; Scrocco, E.; Tomasi, J. *Chem. Phys.* **1981**, *55*, 117–129.
- (66) Miertus, S.; Tomasi, J. *Chem. Phys.* **1982**, *65*, 239–245.

- (67) Klamt, A.; Schüürmann, G. *J. Chem. Soc., Perkin Trans. 2* **1993**, 799, 805.
- (68) Klamt, A. *J. Phys. Chem.* **1995**, 99, 2224–2235.
- (69) Cossi, M.; Rega, N.; Scalmani, G.; Barone, V. *J. Comput. Chem.* **2003**, 24, 669–681.
- (70) Ochterski, J. Vibrational analysis in Gaussian, 1999. Gaussian white papers. http://www.gaussian.com/g_whitepap/vib.htm (accessed Aug 11, 2007).
- (71) Kendall, M. G. The measurement of rank correlation. In *Rank Correlation Methods*; 1st ed.; Charles Griffin and Co.: London, U.K., 1948; pp 8–10.
- (72) Seifert, M. H. J.; Kraus, J.; Kramer, B. *Curr. Opin. Drug Discovery Dev.* **2007**, 10, 298–307.
- (73) Golbraikh, A.; Tropsha, A. *J. Mol. Graphics Modell.* **2002**, 20, 269–276.
- (74) Martens, H. A.; Dardenne, P. *Chemom. Intell. Lab. Syst.* **1998**, 44, 99–121.
- (75) Johnson, R. D., NIST Computational Chemistry Comparison and Benchmark Database, 2005. <http://srdata.nist.gov/cccbdb> (accessed Aug 11, 2007).
- (76) Illingworth, C. J. R.; Gooding, S. R.; Winn, P. J.; Jones, G. A.; Ferenczy, G. G.; Reynolds, C. A. *J. Phys. Chem. A* **2006**, 110, 6487–6497.

CT800404F